Trigonal interactions in holmium

J.A. Simpson
Oxford Physics, Clarendon Laboratory, Parks Road, Oxford OX1 3PU, United Kingdom

D.F. McMorrow
Risø National Laboratory, DK 4000 Roskilde, Denmark

R.A. Cowley and D.A. Jehan
Oxford Physics, Clarendon Laboratory, Parks Road, Oxford OX1 3PU, United Kingdom
(Received 25 October 1994)

The low-temperature magnetic structure of Ho has been studied using a combination of neutron-scattering and mean-field calculations. Reexamination of the cone and one-spin-slip phases has shown that the structures are distorted by interactions of trigonal symmetry, similar to those recently hypothesized for Er. In the cone phase below 18.5 K the moments have two out-of-plane tilt angles with a difference in angle of approximately 1.0° about a mean value of 9.0°. The spin-slip phases are more complex. The moments are modulated with a period twice that of the basic spin-slip structure, giving rise to additional peaks in the scattering. Spin-slip structures found in a *c*-axis field are shown to be consistent with our model. In zero field, the phase transition to the cone phase occurs in two distinct steps, as suggested by anomalies found in several bulk measurements. The intermediate phase has the wave vector locked into $(1/6)\mathbf{c}^*$, where any group of four moments has two tilted in one sense along *c*, and the other two adopt an equal and opposite tilt, resulting in no net *c*-axis moment. Below 18.5 K this arrangement then tilts out of the basal plane, forming the distorted cone structure.

I. INTRODUCTION

Although the underlying nature of the magnetic structures of the heavy rare earths has been known for more than 30 years, there has recently been a renewal of interest in these metals. This has arisen largely from the results of high-resolution x-ray magnetic scattering experiments,[1] which indicated the existence of long-period commensurable phases. Prompted by these findings, subsequent neutron diffraction studies have revealed a wealth of subtleties that were previously undetected, leading to an improvement in our understanding of the magnetic interactions in the heavy rare earths. In this paper we present further refinements to the picture of the magnetic structure of Ho. In particular we show that magnetic interactions of trigonal symmetry exist in Ho, similar to those found in Er,[2] and that they have an important effect on the symmetries of the low-temperature magnetic structures.

The first neutron scattering study of the magnetic structure of Ho was undertaken by Koehler *et al.*,[3] who identified two ordered phases. Between the ordering temperature of 132.2 K and about 18 K, the moments form a basal plane helix: the moments on each sublattice are confined to the basal plane and are ferromagnetically coupled, but the orientation of the moments is rotated on successive sublattices. The wave vector of the helix reduces from $0.271\mathbf{c}^*$ at the onset of magnetic order, to $(1/6)\mathbf{c}^*$ at 18 K. For temperatures below 18 K, the moments tilt out of the basal plane, forming a *c*-axis ferromagnetic cone structure. The presence of fifth- and seventh-order magnetic satellites in the neutron scattering data at low temperatures indicates that the ordering in Ho does not have a constant turn angle between successive planes, and instead the moments are bunched about the nearest easy axis in the basal plane. Felcher *et al.*,[4] and later Pechan and Stassis[5] observed other high-order satellites in their neutron diffraction data, in addition to the fifth- and seventh-order harmonics observed by Koehler *et al.*[3] These peaks showed that the basal-plane ordering is even more complex and cannot be explained by a simple bunched helix. A significant breakthrough in understanding the nature of the distortions giving rise to the higher harmonics was made by Gibbs *et al.*[1] who used the technique of x-ray magnetic scattering to study Ho. The inherent high resolution of this technique revealed that the wave vector does not change smoothly with temperature; below about 30 K the wave vector passes through a series of lock-in transitions to commensurable values, which implies the existence of long-period magnetic structures. To explain these structures, they proposed the spin-slip model of Ho. This model was developed more fully by Cowley and Bates[6] to account for the results of their detailed neutron scattering experiments that revealed many high-order satellites.

The formation of commensurable structures is explicable in terms of the competition between the various interactions in Ho. The stable magnetic structure of Ho is one that minimizes the total energy by attempting to satisfy the exchange and crystal-field energies. Both of

these interactions change with temperature, but whereas the exchange changes only slowly with temperature, the crystal-field energy is more temperature dependent. At the lowest temperatures, the hexagonal anisotropy energy is very large and the moments lie close to the easy axes in the basal plane, with an ordering wave vector of $(1/6)\mathbf{c}^*$. At high temperatures, the hexagonal anisotropy is small and the moments are arranged in a largely undistorted basal-plane helix that has a wave vector determined by the position of the peak in the exchange function, $\mathcal{J}(\mathbf{q})$, and is, in general, incommensurable with the chemical lattice. At intermediate temperatures, when the hexagonal anisotropy and exchange energies have similar magnitudes, compromise arrangements, known as spin-slip structures, are formed. In these, most of the moments are still bunched in pairs about successive easy directions, but there are, at regular intervals, some single moments aligned along an easy axis. These singlets are the spin slips or spin discommensurations. Such an arrangement has all the moments along or close to an easy axis, thereby minimizing the hexagonal-anisotropy energy. By changing the periodicity of the spin slips, an average wave vector may be obtained that is close to the value required by the position of the peak in $\mathcal{J}(\mathbf{q})$. Thus the spacing between successive spin slips changes with temperature, to match the change in the position of the peak of $\mathcal{J}(\mathbf{q})$.

The $(1/6)\mathbf{c}^*$ structure may be regarded as a zero-spin-slip structure, as all the moments are bunched in pairs and there are no singlets. The simplest spin-slip structure has a singlet every 11 planes and a wave vector of $(2/11)\mathbf{c}^*$. In this paper we shall discuss mainly these two phases. To represent the magnetic structures pictorially the directions of successive moments are projected down to a common plane. Figure 1 is a representation of the basal-plane moments in the cone phase and the one-spin-slip phase. In the cone phase the moments are symmetrically bunched about the easy directions, whereas the moments in the doublets of the $(2/11)\mathbf{c}^*$ spin-slip structure are distorted slightly, with all the moments drawn towards the singlet.

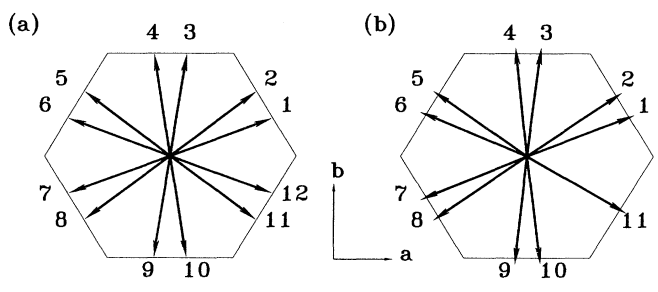

FIG. 1. The basal-plane projections of moments calculated from the crystal-field and exchange parameters of Table I, in the absence of trigonal terms, for (a) $(1/6)\mathbf{c}^*$ and (b) $(2/11)\mathbf{c}^*$ with the number representing the atomic plane of each moment. In (a) the moments have a ferromagnetic component along the c axis, whereas the one-spin-slip phase is confined to the a-b plane. For Ho the easy direction is along b.

The spin-slip model has been highly successful in accounting for the observed neutron scattering from Ho in zero field, and of anomalies in bulk parameters. However, there are features of the magnetic structure that cannot be explained by the simple competition between the anisotropic exchange and crystal-field interactions. For example, Cowley and Bates[6] found evidence for a small oscillating c component to the moment, while the results of a study of the effect of a c-axis field on Ho found evidence of a symmetry breaking between the two sublattices.[7] In addition, the details of the magnetic structure near 18 K are particularly uncertain. As first questioned by Sherrington[8] and subsequently by Felcher *et al.*,[4] there is no reason why the wave vector should lock to $\mathbf{q}= (1/6)\mathbf{c}^*$ at the same temperature as the c-axis moment develops. In principle it is possible that a tilted helix forms before the onset of the cone phase. In addition there is some doubt as to whether the cone angle is as great as was found by Koehler, or whether indeed it exists at all in some Ho samples.[9] Moreover, it has recently been shown that the magnetic structure of Er can be explained only if there are two-ion couplings with a threefold symmetry.[2]

In this paper, we outline the results of a series of experiments to search for evidence of the effects of trigonal couplings, and to investigate the nature of the transition into the cone phase. The following section presents our neutron scattering data which was taken at Risø National Laboratory, Denmark, and in particular inconsistencies between the accepted properties of Ho and certain features of our results are highlighted. Section III outlines the model we have adopted to identify modifications to the magnetic structures, which are considered in Sec. IV. These are found to be considerably more complex than the simple spin-slip model. The nature of the phase transition at 20 K is studied in detail in Sec. V. The trigonal Hamiltonians, which we include in our calculations, and the mean-field model are discussed in the Appendix.

II. EXPERIMENTAL RESULTS

The experiments were performed at the DR3 reactor, Risø National Laboratory, Denmark using the triple-axis spectrometer TAS7. As previous measurements on Ho have highlighted inconsistencies between samples, we have examined two crystals that have been the subject of previous investigations. The smaller of the two was used by Bates *et al.*[10] and is a cylinder of height 3 mm and diameter 5 mm, whereas the larger was used for measurements of the spin waves by McMorrow *et al.*[11] and is $30 \times 12 \times 4$ mm^3. Pyrolitic graphite crystals were used as both monochromator and analyzer, and set to select 5-meV neutrons. A beryllium filter was employed to suppress higher-order contaminent neutrons, which were further attenuated by the curved guide tube to the spectrometer. This also provided a premonochromator collimation of $\approx 30'$. The total horizontal collimation from reactor to detector was set to 30′-37′-60′-open for the small crystal, and 30′-19′-37′-open for the larger, giving wave-vector resolutions of approximately q =0.012 and

0.0097 Å^{-1}, respectively. The samples were mounted in a helium-flow cryostat with the (h 0 ℓ) plane in the scattering plane.

At each temperature scans were performed with the wave-vector transfer **Q** along the [00ℓ] and [10ℓ] directions, at temperatures selected to minimize any phase coexistence. In Fig. 2 we present the results for the large crystal at 10 K in the cone phase. In the context of the currently accepted structure of the cone phase, the most notable features are the peaks marked by the arrows. Along [00ℓ] these peaks occur at $\ell = n \pm \frac{1}{3}$, while along [10ℓ] they are found at $\ell = n \pm \frac{1}{3}$ and $\ell = n + \frac{1}{2}$ where n is an integer. These peaks cannot arise from the simple cone structure of Fig. 1(a). In addition to the regularly spaced peaks in ℓ, broad features are apparent around the $\ell = n \pm \frac{1}{6}$ positions which do not have a constant separation in wave vector. These latter features were also observed using the small crystal, but were not evident in previous measurements[6] made on the same sample using D10 at the Institut Laue Langevin (ILL), as shown in Fig. 3. Although we do not have a detailed explanation of their origin, we believe they are spurious and arise from the poor vertical resolution of TAS7.

For the (2/11)**c*** phase data shown in Fig. 4, weak features are visible at $(00\frac{2n+1}{11})$, and these are again inconsistent with a structure where the moments are confined to the basal plane as illustrated in Fig. 1(b). A further discrepancy is that the previous attempt to model this

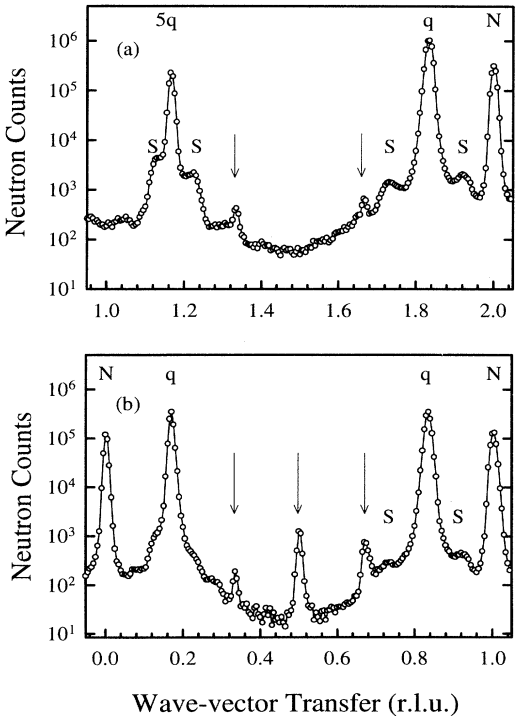

FIG. 2. The neutron scattering data for the large crystal at 10 K with wave-vector transfer along (a) [00ℓ] and (b) [10ℓ]. Peaks marked with the arrows are not accounted for by the undistorted cone structure of Fig. 1(a). The shoulders marked S are not present in the data taken at the ILL, shown in Fig. 3, and the nuclear peaks are labeled N.

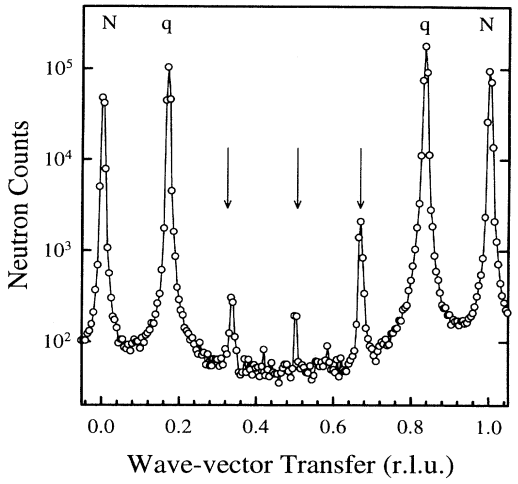

FIG. 3. The neutron scattering data (Ref. 6) taken at the ILL with wave-vector transfer along [10ℓ]. Although this shows the additional features at the $(10\frac{1}{3})$, $(10\frac{2}{3})$, and $(10\frac{1}{2})$ positions with comparable intensities to our data, the features marked S in Fig. 2 are not present.

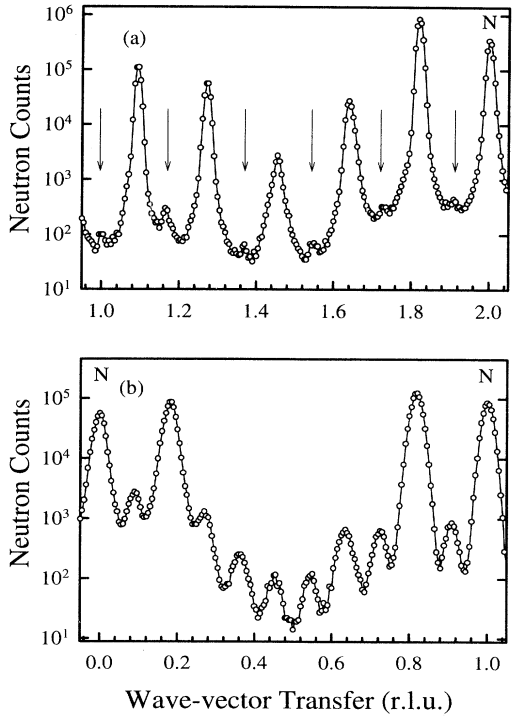

FIG. 4. Neutron scattering data with wave-vector transfer along (a) [00ℓ] for the large crystal and (b) [10ℓ] for the smaller crystal. The temperature, at approximately 20 K, was selected to be such that each sample had a wave vector of (2/11)**c*** without phase coexistence. Peaks marked with an arrow should not be present on the basis of the simple spin-slip model.

phase[6] produced fits predicting intensities smaller than those observed for wave-vector transfers of $(10\frac{5}{11})$ and $(10\frac{6}{11})$. While the general form of the scattering in these two phases is consistent with the structures of Fig. 1, in detail they must be distorted to produce the additional features observed in the scattering.

To study these distortions, Bragg peaks, which are typically 3 orders of magnitude weaker than the nuclear or primary magnetic peaks, must be measured with care in order to obtain reliable integrated intensities. Consequently we have made several tests to assess the integrity of our results. For example, the scattering at $(10\frac{1}{2})$ might be produced by higher-order contaminent neutrons. In our case this is reduced by a cooled Be filter and the curved guide tube to the spectrometer. A useful measure of this effect is to study the (001) position (see Fig. 2), which is a forbidden nuclear reflection for the hcp structure, and should have no contribution from magnetic scattering by a cone-type structure. In our data, there is no observable intensity at this position, and we are confident that our results are not seriously affected by such processes. Other difficulties include multiple scattering and extinction, both of which are more difficult to assess quantitatively. With the two-circle goniometer used in our experiments it is not possible to perform a full Renniger scan[12] to determine the degree of multiple scattering. However, several measurements of (00ℓ) peak intensities were made by tilting the sample around the scattering vector over a range of $\pm 10°$. This produced a negligible change in intensity of the weak peaks. With such difficulties in mind, we have also measured several peaks at different energies between 2 and 5 meV. Since multiple scattering is manifest in different ways as the energy changes, this should enable us to determine if our data are contaminated by multiple scattering. In addition, we have compared our results to a previous study of Ho by Cowley and Bates,[6] taken using the D10 diffractometer at the ILL with 14-meV neutrons. The $[10\ell]$ scans for the cone and $(2/11)\mathbf{c}^*$ phases are shown in Figs. 3 and 5, respectively, and despite being taken at a different neutron energy, they show consistency with our relative intensities to better than a factor of 2. On the basis of these considerations, we can therefore be confident that multiple scattering did not significantly affect our observations. The degree to which extinction affects our results is even more difficult to determine. Unlike either multiple scattering or higher-order contamination, extinction affects only the magnitudes derived for the distortions and not their symmetry. With mosaic spreads of 0.4° and 0.9° for the large and small crystals, respectively, it is likely that the high intensity peaks will be affected by extinction.

Previous x-ray measurements of the charge scattering from Ho have also identified weak features which were ascribed to asphericity in the $4f$ charge density.[13] For a helical structure with wave vector $\mathbf{q}$, these occur at $\boldsymbol{\tau} \pm n\boldsymbol{q}$, where $\boldsymbol{\tau}$ is a reciprocal lattice vector and $n = 1, 2, ..., 6$ for a regular helix and $n = 2, 4, 6$ in the cone phase. While there will be corresponding features in the neutron scattering data, these cannot be responsible for our observations for two reasons: first, the expected intensity is of order 10^{-6} times the primary magnetic peaks, whereas our observations are of order 10^{-3} to 10^{-4}. Second, these features are not present along the $[00\ell]$ direction, where we observe features at $\ell = n \pm \frac{1}{3}$ (n integer). The additional peaks which we observe are therefore magnetic in origin.

To study the nature of the transition to the cone phase,

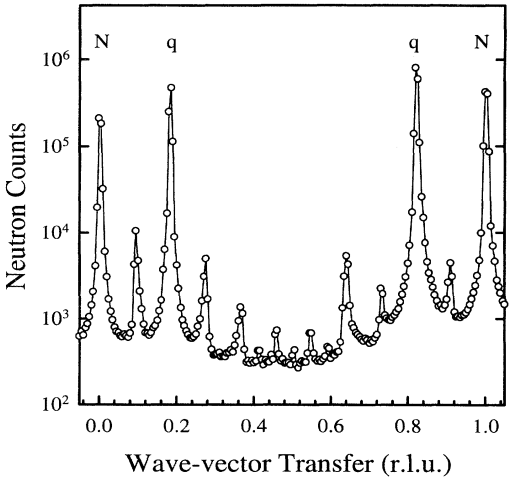

FIG. 5. The neutron scattering data (Ref. 6) taken at the ILL with wave-vector transfer along $[10\ell]$ at 19.7 K.

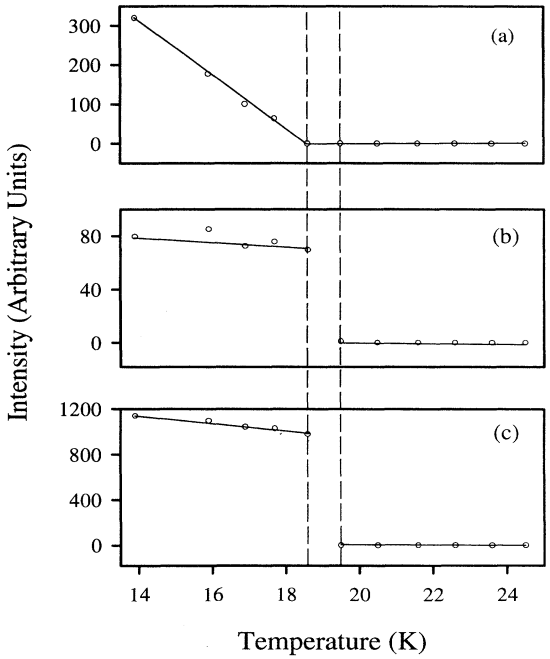

FIG. 6. Integrated intensities of the following peaks: (a) $(10\frac{1}{3})$, (b) $(10\frac{1}{2})$, and (c) $(00\frac{7}{6})$. These measurements were made from the larger crystal on warming, and show a region between the dotted lines where the $(10\frac{1}{3})$ intensity remains constant but that in (b) and (c) does not. Below ≈ 18.5 K the increase in (a) is continuous whereas discontinuities are evident in (b) and (c). The solid lines are guides to the eye.

measurements of the integrated intensities of the $(10\frac{7}{6})$, $(10\frac{1}{2})$, $(10\frac{1}{3})$, and the (100) peaks were taken in temperature steps of approximately 1 K on warming between 15 K and 25 K for the large crystal, and are shown in Fig. 6. Although the transition has been studied previously,[5,14] no measurements have been made of the temperature dependence of the $(10\frac{1}{3})$ peak. As is evident in Fig. 6, this changes in a very different way from the $(10\frac{7}{6})$ or the $(10\frac{1}{2})$ below 20 K. This will be discussed in Sec. V.

III. THE THEORETICAL MODEL

The mean-field model we have used to analyze our data has been developed by Jensen to calculate the magnetic structures of the heavy rare-earth metals.[2,15] The general Hamiltonian is formed from the sum of three terms which, for the ith ion with neighbors j, may be written as

$$\mathcal{H}_0(i) = \mathcal{H}_{\rm cf}(i) + \mathcal{H}_{\rm ex}(i) + \mathcal{H}_{\rm dip}(i) \ , \tag{1}$$

where $\mathcal{H}_{\rm cf}$, the crystal-field interaction, is given by

$$\mathcal{H}_{\rm cf}(i) = \sum_{l=2,4,6} B_l^0 O_l^0(i) + B_6^6 O_6^6(i) \ , \tag{2}$$

the Heisenberg exchange, $\mathcal{H}_{\rm ex}$, by

$$\mathcal{H}_{\rm ex}(i) = -\frac{1}{2}\sum_{ij} \mathcal{J}(ij) \boldsymbol{J_i} \cdot \boldsymbol{J_j} \ , \tag{3}$$

and the dipolar term, $\mathcal{H}_{\rm dip}$, is

$$\mathcal{H}_{\rm dip}(i) = -\frac{1}{2}\sum_{ij} \mathcal{J}_D(ij) J_{zi} J_{zj} \ . \tag{4}$$

In Eqs. (2)–(4), O_l^m are the Stevens operators[16] and B_l^m are the crystal-field parameters, which we have taken from Bohr *et al.*[17] $\mathcal{J}(ij)$ are the real-space exchange constants, the Fourier transform of $\mathcal{J}(\mathbf{q})$, which were determined from spin-wave measurements.[18–20] These parameters are given in Table I, and typically have uncertainties of $\pm 5\%$. A more complete discussion of this Hamiltonian is given by Jensen and Mackintosh.[21]

The Heisenberg exchange of Eq. (3) and dipolar coupling terms in Eq. (4) are both two-ion interactions. For our calculations these are decoupled into expressions containing single-ion operators, and this is achieved using the mean-field approximation. In the Appendix we show how this is applied to the Heisenberg exchange, resulting in Eq. (A7). From the mean-field Hamiltonian, magnetic structures are calculated using a simple iterative procedure. For a commensurable period of N atomic planes, an initial distribution of magnetic moments $\langle \mathbf{J}_j \rangle$ is assumed ($j = 1, 2, \ldots, N$). The mean-field of Eq. (A7) can then be calculated for an ion in the ith plane, and the total Hamiltonian formed in a J_z basis. By diagonalizing this matrix, the partition function and free energy are obtained, and from this a new expectation value $\langle \mathbf{J}_i \rangle$ calculated. This procedure is then repeated for all planes j in the commensurable period, and iterated until self-consistency is achieved.

TABLE I. Crystal-field parameters, B_l^m, and interplanar exchange constants $\mathcal{J}_n$ used in our model for Ho, with units of meV used throughout our calculations.

B_2^0	B_4^0	B_6^0	B_6^6
0.024	0.0	-9.56×10^{-7}	9.21×10^{-6}

J_0	J_1	J_2	J_3	J_4	J_5	J_6
0.3002	0.0895	0.0065	−0.0121	−0.0055	−0.0010	−0.0030

The neutron scattering from these self-consistent structures is then calculated and compared with our data. The elastic scattered-neutron intensity is directly related to the static spin-spin correlation function

$$S_{\alpha\alpha} = \left| \frac{1}{N} \sum_{j=0}^{N-1} \langle J_{\alpha j} \rangle e^{i \boldsymbol{R}_j \cdot \boldsymbol{Q}} \right|^2 \ , \tag{5}$$

where $\mathbf{Q}$ is the wave-vector transfer. Assuming an equal distribution of domains, in which the spiral rotates in a clockwise or anticlockwise sense, the intensity is

$$I(00\ell) = S_{xx}(\boldsymbol{Q}) + S_{yy}(\boldsymbol{Q}) \tag{6}$$

for $\mathbf{Q}$ along $[00\ell]$ and

$$I(10\ell) = (1 - \tfrac{1}{2}\hat{Q}_\perp^2)[S_{xx}(\boldsymbol{Q}) + S_{yy}(\boldsymbol{Q})] + (1 - \hat{Q}_\parallel^2) S_{zz}(\boldsymbol{Q}) \tag{7}$$

for $[10\ell]$. Here $\hat{Q}_\parallel$ and $\hat{Q}_\perp$ are the components of the unit vector $\hat{\boldsymbol{Q}}$ parallel and perpendicular to the c axis. From Eq. (6) it can be seen that the scattering along the $[00\ell]$ direction does not depend on the c-axis component of moments, whereas that along $[10\ell]$ depends on both the basal-plane moment and the c-axis component. Calculating the structure factor from the distribution of moments found above, the intensity is then obtained by including corrections for the form factor and the resolution function of the instrument. The magnetic form factor for a given wave-vector transfer $\mathbf{Q}$ is calculated from the constants tabulated by Brown,[22] and the instrumental resolution using the method of Cowley and Bates.[6] This produces a value proportional to the integrated intensity of peaks measured in scans of $\mathbf{Q}$ along $[00\ell]$ and $[10\ell]$.

The static correlation function of Eq. (5) with $\mathbf{Q}$ parallel to c does not depend on the basal-plane coordinates of the two hexagonal sublattices of the hcp structure. Furthermore, the Hamiltonian $\mathcal{H}_0$ of Eq. (1) does not distinguish between the two sublattices. The consequence of these two facts are most easily realized by considering the scattering from the $(2/11)\mathbf{c}^*$ phase and the cone phase. In the former zero intensity should be observed in scans along $[00\ell]$ when $\ell = (2n+1)/11$ (n integer), and in the latter when $\ell = nq$ (n even). The $[00\ell]$ data for the cone and $(2/11)\mathbf{c}^*$ phases shown in Figs. 2(a) and 4(a),

display weak features, marked by arrows, at these intermediate points indicating that these arguments are incorrect. A possible explanation of this discrepancy is that the Hamiltonian contains terms that distinguish between ions on different sublattices. If these terms have the same form as those described earlier for Er,[2] the Hamiltonian becomes

$$\mathcal{H} = \mathcal{H}_0 + \mathcal{H}_3 \ . \tag{8}$$

Here $\mathcal{H}_3$ are the symmetry breaking terms that are two-ion interactions formed from any linear combination of Stevens' operators,[23] subject to the restriction of time-reversal symmetry and $\mathcal{H}_3$ being Hermitian. A discussion of these restrictions and the terms that are then allowed are given in the Appendix. The terms of lowest order not already present in $\mathcal{H}_0$ are $\mathcal{H}_{31}^{21}$, $\mathcal{H}_{31}^{30}$, and $\mathcal{H}_{22}^{21}$, denoted by the order of the Stevens' operators of which they are comprised. These are all of *trigonal* rather than *hexagonal* symmetry, and we label the interplanar coupling constants $\mathcal{K}_{ll'}^{mm'}(n)$ in each case. In our model we have considered interactions out to the third nearest neighbors, i.e., $n = 1, 2, 3$ only. These terms of trigonal symmetry have been required to describe other properties of the rare earths. In the case of Tb they were introduced to account for the strong interaction between the acoustic magnons and optical transverse phonons.[24] They were also necessary to describe the magnetic structures found in Er,[2] where the typical contribution of the trigonal couplings to the free energy was a factor of 100 smaller than the exchange terms.

Using mean-field theory, these trigonal terms are decoupled in a similar way to the Heisenberg exchange. This is described in detail for each term by Eqs. (A2)–(A4) in the Appendix. We have modeled our neutron scattering data by considering the effect on the structure of each of these terms in turn. A limitation of the model is that many configurations of moments may be produced, dependent on the initial configuration of $\langle \mathbf{J}_j \rangle$ chosen. In most situations the naturally occurring structure is easily identified as that with the lowest free energy, and for the case of the Hamiltonian $\mathcal{H} = \mathcal{H}_0$, there are large energy differences between the possible structures (≈ 1 meV is typical). In some other cases, the calculated structure is clearly inconsistent with our neutron scattering data. However, when the trigonal terms $\mathcal{H}_3$ are included in the Hamiltonian, it is more difficult to choose the appropriate structure as several similar structures are formed, all of which are slightly different modifications of the basic structures of Fig. 1, and produce very similar neutron scattering patterns. This makes a precise determination of the structure difficult, and the following section discusses a range of possible modifications to the cone and spin-slip phases.

IV. MAGNETIC STRUCTURES

We have shown in Sec. II that the neutron scattering data for Ho has several features that are inconsistent with the symmetry of the Hamiltonian $\mathcal{H} = \mathcal{H}_0$, and indicated the need for interactions which distinguished between the two sublattices of the hcp structure. In this section, possible modifications to the structures of the cone and spin-slip phases are presented. We find that the inclusion of the $\mathcal{H}_{31}^{21}$ trigonal term gives a consistent description of our experimental data, using the coupling constants of Table II. For the remaining terms $\mathcal{H}_{31}^{30}$ and $\mathcal{H}_{22}^{21}$, we were unable to find a unique set of coupling constants that provided a satisfactory fit to the data, although the type of modifications to the basic structures are the same. This was also found to be the case in the case of Er.[2]

TABLE II. The trigonal parameters $\mathcal{K}_{31}^{21}(n)$ which give satisfactory fits to our data. These values are uncertain to ± 0.00003.

$n = 1$	2	3
0.00030	0.00022	-0.00022

To add further confidence to our modeling of the structures, we have also reexamined the data for Ho in a c-axis magnetic field.[7] Here we shall restrict ourselves to the cases of the $(2/11)\mathbf{c}^*$ and $(3/16)\mathbf{c}^*$ phases produced at $T = 4$ K, $B_c = 2$ T, and $T = 17$ K, $B_c = 4$ T, respectively. The results from our model are generally in good agreement with the experimental intensities, and clarify the complex nature of the magnetic structures of Ho found in an applied field.

A. The cone phase

The observation of peaks at $\ell = n \pm \frac{1}{3}$ for scans of the wave-vector transfer along $[00\ell]$ and $[10\ell]$ indicates a modulation of the $\mathbf{q}=(1/6)\mathbf{c}^*$ basal-plane structure with a period of two unit cells. The additional $(10\frac{1}{2})$ peak, but no corresponding $(00\frac{1}{2})$ scattering, is indicative of an antiferromagnetic component to the moments along c with the same period. Modifications to the cone consistent with these features would be one in which the out-of-plane tilt was not in fact constant, but oscillated with a period of two unit cells (four atomic planes). The introduction of $\mathcal{H}_{31}^{21}$ produces the structure shown in Fig. 7(a), where alternate pairs of moments have the same out-of-plane tilt, but the intermediate pairs have a smaller value. Since the total moment length is constant at low temperatures, the basal-plane projections also vary in this manner. In addition the B_6^6 crystal-field term causes slightly different bunching angles for successive pairs. We obtain a difference of 1.6°, although this is not shown to scale in Fig. 7(a). The results of the fits to the scattering are shown in Figs. 8(a) and 8(b).

The cone angle of Ho has been the subject of many experiments since the initial values of 10.2° and 9.8° measured for samples A and B by Koehler.[3] Subsequent measurements have generally found values slightly smaller but broadly consistent with Koehler's values, for example 9.5° by Pechan[5] and 9.8° by Felcher.[4] We have repeated the measurement of the (100) intensity, but in addition we have studied the $(10\frac{1}{2})$ peak, to investigate the av-

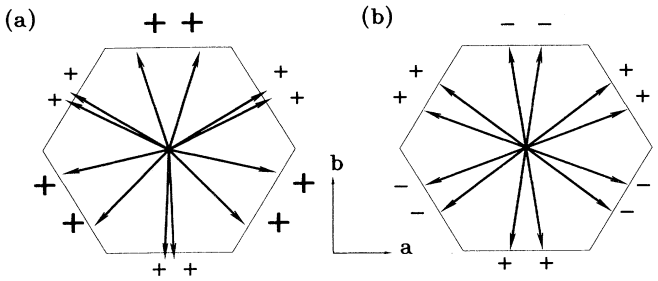

FIG. 7. (a) Modifications to the cone phase of Fig. 1(a) produced by the trigonal terms $\mathcal{H}_{31}^{21}$. The pairs with a large tilt are marked +, and the smaller tilt denoted +; these are the same sense along c. The difference in tilt also causes a different in bunching angles, however this is shown on an exaggerated scale. In (b) the tilt for bunched pairs alternates between two equal and opposite value; this is formed near the phase transition at 20 K.

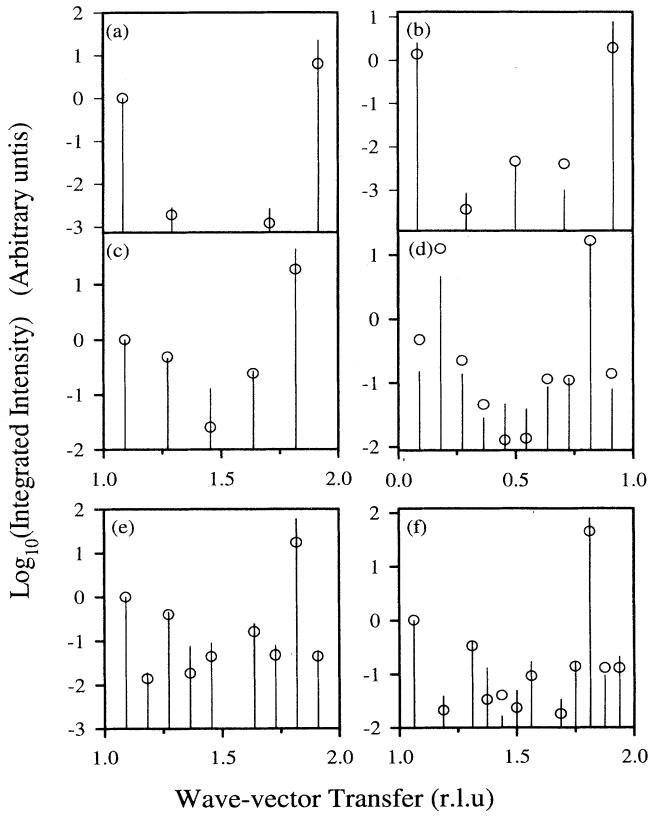

FIG. 8. Comparison of the measured integrated intensities in the cone phase (open circles) to the modeled magnetic structures (vertical lines) for the structures discussed in Sec. IV: (a) and (b) from the large crystal in the cone phase with wave-vector transfer along $[00\ell]$ and $[10\ell]$, respectively. (c) and (d) are the corresponding results from the small crystal for the $(2/11)\mathbf{c}^*$ phase in zero field. The remaining data are with a c-axis field for $\mathbf{Q}$ along $[00\ell]$: (e) $B_C = 2$ T, $T = 4$ K, again in the $(2/11)\mathbf{c}^*$ phase, and (f) $B_C = 4$ T, $T = 17$ K with $\mathbf{q}=(3/16)\mathbf{c}^*$.

erage cone angle and separation between the large and small tilts. For either of the structures in Fig. 7, if the c-axis moments can adopt a value of J or J', the scattering at (100) is proportional to the square of $(J + J')/2$, and that at $(10\frac{1}{2})$ depends on $(J - J')^2$. Correcting these for the form factor and resolution effects, and assuming a random domain distribution, the results suggest an average out-of-plane tilt of 9.0° and a difference between the tilting of 1.0° for the small crystal, while our free energy calculations give values of 10.5° and 1.4°, respectively.

B. The (2/11)c* phase

The scattering from the $(2/11)\mathbf{c}^*$ phase in zero field has features similar to the data from the cone phase, as discussed in Sec. II. We have modeled this phase by taking the integrated intensities of all peaks except those given by $(00\frac{2n+1}{11})$, since although Fig. 4(a) shows peaks at these points, they are too weak to extract accurate structure factors from. Using the trigonal coupling constants of Table II, the modifications from $\mathcal{H}_{31}^{21}$ are more complex than those of the cone phase, and the configuration produced is shown in Table III. The fit to the scattering from this structure is shown in Figs. 8(c) and 8(d).

In view of the difficulties associated with measuring the scattering at $(00\frac{2n+1}{11})$ for the zero-field case, we have reexamined the data for Ho in a c-axis field[7] where they are relatively stronger. At a temperature of 4 K and $B_C = 2T$, the $(2/11)\mathbf{c}^*$ phase is again formed, but the moments now have a larger out-of-plane tilt. The scat-

TABLE III. Calculations of the basal-plane and c-axis components of the $(2/11)\mathbf{c}^*$ phase at $T = 20$ K using the trigonal constants $\mathcal{K}_{31}^{21}$ given in Table II. The turn angle is also given, and is determined with respect to the b axis.

Plane	J_{ab}	J_c	Turn angle
1	9.69	-1.25	-10.4
2	9.78	-1.17	6.1
3	9.80	-0.41	52.7
4	9.82	0.01	66.5
5	9.81	-0.07	113.0
6	9.81	-0.07	127.0
7	9.82	0.01	173.5
8	9.80	-0.41	187.3
9	9.78	-1.17	233.9
10	9.69	-1.25	250.4
11	9.85	0.00	300.0
12	9.69	1.25	-10.4
13	9.78	1.17	6.1
14	9.80	0.41	52.7
15	9.82	-0.01	66.5
16	9.81	0.07	113.0
17	9.81	0.07	127.0
18	9.82	-0.01	173.5
19	9.80	0.41	187.3
20	9.78	1.17	233.9
21	9.69	1.25	250.4
22	9.85	0.00	300.0

tering at $(00\frac{2n+1}{11})$ is now of comparable intensity to the other peaks along $[00\ell]$, and a proper fit, sensitive to the basal-plane behavior, can now be performed. Previous fits to this phase predicted zero intensity at the $(00\frac{2n+1}{11})$ positions,[9] whereas we have found very good agreement when $\mathcal{H}_{31}^{21}$ is included in the model, as shown in Fig. 8(e). The structure is modulated in a similar way to the zero-field case, but has a larger net component along c.

C. The (3/16)c* phase

The application of a c-axis field to Ho produced several spin-slip structures not exhibited in the bulk, one of which has $\mathbf{q} = (3/16)\mathbf{c}^*$ phase. This is formed from a sequence of three pairs, a singlet, four pairs, and a final singlet. Due to the two hcp sublattices, the true periodicity is 32 atomic planes, and it would be expected for this unit of 16 moments to repeat in a regular manner, i.e. the moments would follow a (7979) sequence. In their study of this phase, Cowley *et al.*[7] explained the existence of peaks at $(00\frac{2n}{16})$ by proposing the 32-plane period instead followed a (7997) configuration, since a regular (7979) structure cannot produce this scattering in the absence of the trigonal terms. We have considered the effect of trigonal terms on the basic (7979) arrangement, and the results give scattering at the additional values of ℓ, and consistency is obtained for $\mathcal{H}_{31}^{21}$, as shown in Fig. 8(f). On the basis of this success in accounting for the previously considered structures of Ho, we conclude that a more suitable description of this phase is one where the basic (7979) structure has a modulation in the c axis and corresponding basal-plane component with a period of two unit cells, of a similar nature to the distortions of the $(2/11)\mathbf{c}^*$ structure.

V. THE TRANSITION AT 20 K

The transition at 20 K has been the subject of several previous experiments. Measurements of the specific heat of Ho (Ref. 25) have identified two anomalies close to 20 K, with a first-order phase transition occurring at 19.5 K followed by a second-order one at 17.3 K. Other bulk measurements, such as ultrasonics, have indicated two features in the vicinity of 20 K, with measurements of the elastic constants C_{11}, C_{33}, and C_{44} all showing anomalies at 17.8 K and 19.5 K.[10] Although these results are somewhat sample dependent, and exhibit a 1–2 K hysteresis, they indicate that there are two transitions. One possibility is that on cooling the wave vector first locks into $(1/6)\mathbf{c}^*$ through a first-order transition, and a that subsequent second-order transition occurs $\approx$2 K lower. We have made measurements of the temperature dependence of the scattering at several points in reciprocal space to determine the exact sequence of phase transitions: the appearance of scattering at $(10\frac{7}{6})$ identifies the transition to a wave vector of $(1/6)\mathbf{c}^*$, whereas that at $(10\frac{1}{3})$ indicates any basal-plane modulation of the moment length. To study the c-axis components, the (100) intensity gives the net ferromagnetic component along c, whereas the $(10\frac{1}{2})$ is a measure of the antiferromagnetic moment. A summary of these results is given in Fig. 6. They indicate that the wave vector first locks into $(1/6)\mathbf{c}^*$ at 19.5 K, with the c-axis antiferromagnetic moment developing its saturation value at the same temperature. In contrast, the temperature dependence of the $(10\frac{1}{3})$ peak indicates that the basal-plane projections of the spiral are constant until $\approx$18.5 K, and that the modulations gradually develop below this temperature.

Considering the structure between 18.5 K and 19.5 K, we have used our model to calculate the possible structures that can be formed when $\mathbf{q}=(1/6)\mathbf{c}^*$ as the temperature is raised. Using the constants of Table II, the structure of Fig. 7(b) is produced, where successive pairs of moments have equal and opposite tilt angles (hence constant basal-plane projections). This is attained at a temperature of 25 K, slightly higher than observed. However, mean-field theory invariably overestimates critical temperatures, and we conclude that the structure in this small temperature region is one where any group of four moments contain two with a tilt "up" along c, whereas the other two have an equal tilt "down." This gives rise to the antiferromagnetic modulation, but still retains a constant in-plane component.

Below 18.5 K, the rise in the (100) intensity indicates a ferromagnetic component developing along c, and the "two-up–two-down" structure must lift out of the basal plane. Due to the unequal tilts of individual moments, differences in the basal-plane projections develop, and this produces scattering at $(10\frac{1}{3})$. The antiferromagnetic component of the c-axis moments must remain constant, as the intensity of the $(10\frac{1}{2})$ does not change below 18.5 K, and as discussed in Sec. IV, the average out-of-plane tilt at 10 K was measured to be 9.0° with an opening angle of 1.0°.

The transition to the low temperature cone structure therefore occurs in two distinct steps: first, the wave vector locks into $(1/6)\mathbf{c}^*$ where the moments have a "two-up–two-down" arrangement. Below 18.5 K this cants out of the plane forming a modulated cone structure where there are two possible values of tilt.

VI. SUMMARY

We have shown that the neutron scattering from Ho at low temperatures cannot be reconciled with its currently accepted magnetic structure. A good description of the additional features we observe in the scattering is obtained if two-ion terms of trigonal symmetry are included in the mean-field Hamiltonian. Of the three possible lowest-order trigonal interactions, we find that the term $\mathcal{H}_{31}^{21}$ provides the only consistent account of our data for interactions extending out to third-nearest neighbors. The magnitude of the constants $\mathcal{K}_{31}^{21}(n)$ are of order 0.0001 meV (see Table II), and are of comparable magnitude to those used in Er.[2] Including $\mathcal{H}_{31}^{21}$ in the Hamiltonian modifies the cone and spin-slip structures to produce c-axis modulations, which have a periodicity of two unit cells (four atomic planes), with corresponding

variations in the basal-plane projections.

The phase transition from the $(2/11)\mathbf{c}^*$ to the cone phase is found to occur via an intermediate phase that exists over a narrow temperature range from approximately 19.5 K to 18.5 K. In this interval the moments adopt a "two-up–two-down" configuration with no net moment. This then tilts out of the basal plane on cooling below 18.5 K to form a ferromagnetic cone.

The data presented in this paper illustrate the importance of the trigonal terms on the low-temperature magnetic structures of Ho. The trigonal terms were first used to account for the strong interaction found between the acoustic magnons and optical transverse phonons in Tb,[24] and were subsequently invoked to explain the complex magnetic structures formed in Er.[2] They may well be present in all of the heavy rare-earth metals. Although these terms are postulated to arise from a spin-orbit coupling of the conduction electrons,[2] we have as yet no detailed understanding of their microscopic origin.

ACKNOWLEDGMENTS

We would like to thank Jens Jensen for invaluable help with the model, and we have also benefited from discussions with Allan Mackintosh. The experimental work at Risø was funded by the EU through the Large Installation Programme and the work in Oxford by the EPSRC. We would also like to express our thanks to G. McIntyre and S. Bates for making their ILL data available.

APPENDIX: TRIGONAL INTERACTIONS

In this appendix we discuss the form of the trigonal terms in the Hamiltonian and how they may be treated within mean-field theory. Although similar considerations have been made by Cowley and Jensen,[2] only the term $\mathcal{H}_{31}^{21}$ was dealt with in detail. For completeness we shall consider the three possible trigonal terms of lowest order.

For a rare-earth element, satisfying time-reversal symmetry and for a Hermitian Hamiltonian, any interaction between atoms in planes i and j will produce a term in the Hamiltonian of the form

$$\mathcal{H} = \sum_{ij} \tilde{K_{ll'}^{mm'}}(ij)\tilde{O}_l^m(i)\tilde{O}_{l'}^{m'}(j) + (-1)^{m+m'}\tilde{K_{ll'}^{mm'}}(ij)^*\tilde{O}_l^{-m}(i)\tilde{O}_{l'}^{-m'}(j) \ . \quad \text{(A1)}$$

In this equation, $\tilde{O}_l^m$ are the Racah operators, which are formed from linear combinations of the corresponding Stevens' operators O_l^{-m} and O_l^m.[23] The Racah operators have the advantage of simple transformation properties under rotations of the coordinate frame, and an operator denoted by (l,m) would be formed from the spherical harmonics Y_l^m. For the hcp structure, consisting of two hexagonal sublattices, the c axis is a threefold axis of symmetry, and Eq. (A1) must be invariant under rotations of $2\pi/3$. This restricts us to considering terms with $m+m' = 3p$ $(p = 0,1,2,...)$ and the operators are also required to have $l+l' \geq m+m'$. The coupling constants $K_{ll'}^{mm'}(ij)$ are constrained so as to be wholly real.

Equation (A1) encompasses terms already in the Hamiltonian $\mathcal{H}_0$ of Eq. (1), and those with $p=0$ include the Heisenberg exchange and the axial crystal-field. The hexagonal crystal-field term has $p=2$, but there are no terms included in $\mathcal{H}_0$ with $p=1$. Choosing terms of lowest order, i.e., $l+l'=4$, there are three possible terms, $\tilde{H}_{22}^{21}$, $\tilde{H}_{31}^{30}$, and $\tilde{H}_{31}^{21}$, and these are given in terms of the Stevens' operators as

$$\mathcal{H}_{31}^{21}(i) = \sum_{ij} \mathcal{K}_{31}^{21}(ij)\left[O_3^2(i)J_{yj} + O_3^{-2}(i)J_{xj}\right] \ , \quad \text{(A2)}$$

$$\mathcal{H}_{31}^{30}(i) = \sum_{ij} \mathcal{K}_{31}^{30}(ij)O_3^{-3}(i)J_{zj} \ , \quad \text{(A3)}$$

$$\mathcal{H}_{22}^{21}(i) = \sum_{ij} \mathcal{K}_{22}^{21}(ij)\left[O_2^2(i)O_2^{-1}(j) + O_2^{-2}(i)O_2^1(j)\right] \ . \quad \text{(A4)}$$

These equations contain two-ion terms, and the mean-field approximation is used to decouple these into a single-ion form. Considering the simpler example of the Heisenberg exchange,

$$\mathcal{H} = -\frac{1}{2}\sum_{ij} \mathcal{J}(ij)\boldsymbol{J}_i \cdot \boldsymbol{J}_j \ , \quad \text{(A5)}$$

the two-ion operator $\boldsymbol{J}_i \cdot \boldsymbol{J}_j$ is expanded as

$$\boldsymbol{J}_i \cdot \boldsymbol{J}_j = (\boldsymbol{J}_i - \langle \boldsymbol{J}_i \rangle)\cdot(\boldsymbol{J}_j - \langle \boldsymbol{J}_j \rangle) + \boldsymbol{J}_i \cdot \langle \boldsymbol{J}_j \rangle + \boldsymbol{J}_j \cdot \langle \boldsymbol{J}_i \rangle - \langle \boldsymbol{J}_i \rangle \cdot \langle \boldsymbol{J}_j \rangle \ . \quad \text{(A6)}$$

In the mean-field approximation the first term on the right-hand side, which is associated with two-site fluctuations, is neglected, and the Hamiltonian can then be written as

$$\mathcal{H} = (\boldsymbol{J}_i - \tfrac{1}{2}\langle \boldsymbol{J}_i \rangle)\cdot \sum_j \mathcal{J}(ij)\langle \boldsymbol{J}_j \rangle \ . \quad \text{(A7)}$$

The term $\sum_j \mathcal{J}(ij)\langle \boldsymbol{J}_j \rangle$ is referred to as the "mean field" at the ith site, and the term involving $\frac{1}{2}\langle \boldsymbol{J}_i \rangle$ is a correction to avoid double counting. Decoupling Eqs. (A2)–(A4) in this manner the following expressions are obtained. From Eq. (A2),

$$\begin{aligned}\mathcal{H}_{31}^{21}(i) = (-1)^s \sum_{n\geq 1} \left[\mathcal{K}_{31}^{21}(n)\right] &\left[\{O_3^2(s) - \tfrac{1}{2}\langle O_3^2(s)\rangle\}\langle J_y(s+n) - J_y(s-n)\rangle \right.\\ &+\{O_3^{-2}(s) - \tfrac{1}{2}\langle O_3^{-2}(s)\rangle\}\langle J_x(s+n) - J_x(s-n)\rangle - (-1)^n\{J_{ys} - \tfrac{1}{2}\langle J_{ys}\rangle\}\langle O_3^2(s+n) - O_3^2(s-n)\rangle \\ &\left.-(-1)^n\{J_{xs} - \tfrac{1}{2}\langle J_{xs}\rangle\}\langle O_3^{-2}(s+n) - O_3^{-2}(s-n)\rangle\right] \quad \text{(A8)}\end{aligned}$$

and from Eq. (A3),

$$\mathcal{H}_{31}^{30}(s) = (-1)^s \sum_{n\geq 1} [\mathcal{K}_{31}^{30}(n)] \, [\, (-1)^n \{J_{zs} - \tfrac{1}{2}\langle J_{zs}\rangle\}\langle O_3^{-3}(s+n) - O_3^{-3}(s-n)\rangle$$
$$-(-1)^n \, \{O_3^{-3}(s) - \tfrac{1}{2}\langle O_3^{-3}(s)\rangle\}\langle J_y(s+n) - J_y(s-n)\rangle \,] \, . \tag{A9}$$

Finally, from Eq. (A4)

$$\mathcal{H}_{22}^{21}(s) = (-1)^s \sum_{n\geq 1} [\mathcal{K}_{22}^{21}(n)] \, [\{O_2^2(i) - \tfrac{1}{2}\langle O_2^2(s)\rangle\}\langle O_2^{-1}(s+n) - O_2^{-1}(s-n)\rangle$$
$$+\{O_2^{-2}(s) - \tfrac{1}{2}\langle O_2^{-2}(s)\rangle\}\langle O_2^1(s+n) - O_2^1(s-n)\rangle - (-1)^n\{O_2^1 - \tfrac{1}{2}\langle O_2^1\rangle\}\langle O_2^{-2}(s+n) - O_2^{-2}(s-n)\rangle$$
$$-(-1)^n\{O_2^1 - \tfrac{1}{2}\langle O_2^1\rangle\}\langle O_2^{-2}(s+n) - O_2^{-2}(s-n)\rangle \,] \, . \tag{A10}$$

In the above equations, s refers to an ion in the ith plane and the summation is done over an atom n planes away. We have restricted ourselves to considering interactions up to third-nearest neighbors; i.e., n=1,2,3 only.

[1] D. Gibbs, D.E. Moncton, K.L. D'Amico, J. Bohr, and B.H. Grier, Phys. Rev. Lett. **55**, 234 (1985).
[2] R.A. Cowley and J. Jensen, J. Phys. Condens. Matter **4**, 9673 (1992).
[3] W.C. Koehler, J.W. Cable, M.K. Wilkinson, and F.O. Wollan, Phys. Rev. **151**, 414 (1966).
[4] G.P. Felcher, G.H. Lander, T. Ari, S.K. Sinha, and F. H. Spedding, Phys. Rev. B **13**, 3034 (1976).
[5] M.J. Pechan and C. Stasis, J. Appl. Phys. **55**, 1900 (1984).
[6] R.A. Cowley and S. Bates, J. Phys. C **21**, 4113 (1988).
[7] R.A. Cowley, D.A. Jehan, D.F. McMorrow, and G.J. McIntyre, Phys. Rev. Lett. **66**, 1521 (1991).
[8] D. Sherrington, Phys. Rev. Lett. **28**, 364 (1971).
[9] D.A. Jehan, Ph.D. thesis, University of Oxford, 1993 (unpublished).
[10] S. Bates, C. Patterson, G.J. McIntyre, S.B. Palmer, A. Mayer, R.A. Cowley, and R. Melville, J. Phys. C **21**, 4125 (1988).
[11] D.F. McMorrow, C. Patterson, H. Godfrin, and D.A. Jehan, Europhys. Lett. **15**, 541 (1991).
[12] M. Renniger, Z. Phys. **106**, 141 (1937).
[13] D. T. Keating, Phys. Rev. **178**, 732 (1969).
[14] A.S. Pearce, Ph.D. thesis, University of Warwick, 1991 (unpublished).
[15] J. Jensen, J. Phys. F **6**, 1145 (1976).
[16] M.T. Hutchings, Solid State Phys. **16**, 227 (1964).
[17] J. Bohr, D. Gibbs, J.D. Axe, D.E. Moncton, K.L. D'Amico, C.F. Majkrzak, J. Kwo, M. Hong, C.L. Chien, and J. Jensen, Physica B **159**, 93 (1989).
[18] C.C. Larsen, J. Jensen, and A.R. Mackintosh, Phys. Rev. Lett. **59**, 712 (1987).
[19] J. Jensen (private communication).
[20] A.R. Mackintosh and J. Jensen, in *Disorder in Condensed Matter Physics*, edited by J.A. Blackman and J. Taguena (Oxford University Press, New York, 1990), Chap. 15.
[21] J. Jensen and A.R. Mackintosh, *Rare Earth Magnetism—Structures and Excitations* (Oxford University Press, New York, 1991).
[22] J. Brown, *International Tables for Crystallography* (Dordecht, Holland, 1983), Vol. C.
[23] P.A. Lindgård and O. Danielsen, J. Phys. C **7**, 1523 (1974).
[24] J. Jensen and J.G. Houmann, Phys. Rev. B **12**, 320 (1975).
[25] A.M. Stewart and S.J. Collocott, J. Phys. Condens. Matter **1**, 677 (1989).
[26] D.A. Tindall, M.O. Steinitz, M. Kahrizi, D.R. Noakes, and N. Ali, J. Appl. Phys. **69**, 5691 (1991).